INTERNATIONAL JOURNAL FOR NUMERICAL METHODS IN FLUIDS, VOL. 16, 447–459 (1993)

SURFACE WAVES PROPAGATION IN SHALLOW WATER: A FINITE ELEMENT MODEL

J. S. ANTUNES DO CARMO AND F. J. SEABRA SANTOS

Faculdade de Ciências e Tecnologia, Universidade de Coimbra, 3049 Coimbra Codex, Portugal

AND

E. BARTHÉLEMY

Institut de Mécanique de Grenoble, BP53x – 38041 Grenoble Cedex, France

SUMMARY

A two-dimensional (in-plane) numerical model for surface waves propagation based on the non-linear dispersive wave approach described by Boussinesq-type equations, which provide an attractive theory for predicting the depth-averaged velocity field resulting from that wave-type propagation in shallow water, is presented. The numerical solution of the corresponding partial differential equations by finite-difference methods has been the subject of several scientific works. In the present work we propose a new approach to the problem: the spatial discretization of the system composed by the Boussinesq equations is made by a finite element method, making use of the weighted residual technique for the solution approach within each element. The model is validated by comparing numerical results with theoretical solutions and with results obtained experimentally.

KEY WORDS Shallow water Boussinesq equations Finite element method Solitary wave

1. INTRODUCTION

The knowledge of the flow characteristics associated with waves, tides and currents and its dependence relative to coastal geometry is of vital concern to coastal work, to forecast the consequent modifications on established agitation and for the movement of coastal sediment.

It is well known that only a non-linear dispersive wave theory is able to represent rigorously the long-term history of real flows in shallow-water conditions.

For the solution of non-linear dispersive waves described by Boussinesq-type equations, several finite-difference methods in one space dimension have been used.[1–5] However, in finite element methods both in one and two space dimensions, the solution of these equations is extremely limited, and that which is available is restricted, in so far as is known by the writers, to a horizontal bottom.[6]

The purpose of this paper is to present an alternative approach to the several developed models, based on the finite element method, to obtain the numerical solution of the Boussinesq-type equations in a domain with arbitrary bathymetry and any geometry.

0271–2091/93/060447–13$11.50

Received February 1992
Revised October 1992

2. FORMULATION

Taking into account the stresses at the bed, an extension of the Boussinesq equations may be obtained from the fundamental equations of the fluid mechanics relating to a three-dimensional and quasi-irrotational flow of a viscous fluid.

Proceeding by suitable dimensionless variables of these equations, written in Euler's variables, and defining the dimensionless quantities $\varepsilon = A/h_0$ and $\sigma = h_0/l$, in which A is a characteristic wave amplitude, h_0 is the mean water depth and l is a characteristic length, we obtain the continuity equation.

Accepting, after that, the fundamental hypothesis of the shallow-water theory ($h_0/l \ll 1$) and developing the dependent variables in power series of the small parameter σ^2 we obtain, after some algebraic manipulations, the momentum equations in second approach (order 2 in σ^2).

Finally, assuming that the ratio of a typical measure of the wave height A to the mean water depth h_0 is small, i.e. with the relative elevation of the surface due to the waves having a value close to the square of the relative depth,

$$\frac{A}{h_0} \approx \left(\frac{h_0}{l}\right)^2 \Rightarrow U = \frac{Al^2}{h_0^3} \approx 1,$$

where U is the Ursell number, we obtain, with dimensional variables and accepting a time-invariable bathymetry, the following governing equation system:[7]

$$h_t + (h\bar{u})_x + (h\bar{v})_y = 0,$$

$$\bar{u}_t + \bar{u}\bar{u}_x + \bar{v}\bar{u}_y + g(h_x + \xi_x) - \frac{(H-\xi)^2}{3}(\bar{u}_{xxt} + \bar{u}_{yyt}) - \frac{(H-\xi)}{2}(H-\xi)_{xx}\bar{u}_t - (H-\xi)(H-\xi)_x\bar{u}_{xt}$$

$$- \frac{(H-\xi)}{2}(H-\xi)_y\bar{u}_{yt} - \frac{(H-\xi)}{2}(H-\xi)_x\bar{v}_{yt} - \frac{(H-\xi)}{2}(H-\xi)_{xy}\bar{v}_t - \nu(\bar{u}_{xx} + \bar{u}_{yy}) + \tau x(\xi) = 0, \qquad (1)$$

$$\bar{v}_t + \bar{u}\bar{v}_x + \bar{v}\bar{v}_y + g(h_y + \xi_y) - \frac{(H-\xi)^2}{3}(\bar{v}_{xxt} + \bar{v}_{yyt}) - \frac{(H-\xi)}{2}(H-\xi)_{yy}\bar{v}_t - (H-\xi)(H-\xi)_y\bar{v}_{yt}$$

$$- \frac{(H-\xi)}{2}(H-\xi)_x\bar{v}_{xt} - \frac{(H-\xi)}{2}(H-\xi)_y\bar{u}_{xt} - \frac{(H-\xi)}{2}(H-\xi)_{xy}\bar{u}_t - \nu(\bar{v}_{xx} + \bar{v}_{yy}) + \tau_y(\xi) = 0,$$

in which h is the total water depth, H the initial water level, $\bar{u}$ the dimensional horizontal mean velocity throughout the Ox direction, $\bar{v}$ the dimensional horizontal mean velocity throughout the Oy direction, ξ the bed elevation, t the dimensional time and x and y are dimensional distances.

3. NUMERICAL MODEL

The numerical model is based on the finite element method for the spatial discretization of the partial differential equations, making use of the weighted residual technique for the solution approach within each element.

3.1. Numerical procedure

Grouping the derivatives in time of the momentum equations in a single term, equation system (1) takes the following form:

$$h_t + h\bar{u}_x + \bar{u}h_x + h\bar{v}_y + \bar{v}h_y = 0,$$

$$r_t = -\bar{u}\bar{u}_x - \bar{v}\bar{u}_y - g(h_x + \xi_x) + \nu(\bar{u}_{xx} + \bar{u}_{yy}) - \tau x(\xi),$$

$$s_t = -\bar{u}\bar{v}_x - \bar{v}\bar{v}_y - g(h_y + \xi_y) + \nu(\bar{v}_{xx} + \bar{v}_{yy}) - \tau y(\xi),$$

$$\bar{u} - \frac{(H-\xi)^2}{3}(\bar{u}_{xx} + \bar{u}_{yy}) - \frac{(H-\xi)}{2}(H-\xi)_{xx}\bar{u} - (H-\xi)(H-\xi)_x\bar{u}_x$$

$$- \frac{(H-\xi)}{2}(H-\xi)_y\bar{u}_y - \frac{(H-\xi)}{2}[(H-\xi)_x\bar{v}_y + (H-\xi)_{xy}\bar{v}] = r, \tag{2}$$

$$\bar{v} - \frac{(H-\xi)^2}{3}(\bar{v}_{xx} + \bar{v}_{yy}) - \frac{(H-\xi)}{2}(H-\xi)_{yy}\bar{v} - (H-\xi)(H-\xi)_y\bar{v}_y$$

$$- \frac{(H-\xi)}{2}(H-\xi)_x\bar{v}_x - \frac{(H-\xi)}{2}[(H-\xi)_y\bar{u}_x + (H-\xi)_{xy}\bar{u}] = s,$$

where $\tau x(\xi) = g\bar{u}\sqrt{(\bar{u}^2 + \bar{v}^2)}/(k^2 h^{4/3})$ and $\tau y(\xi) = g\bar{v}\sqrt{(\bar{u}^2 + \bar{v}^2)}/(k^2 h^{4/3})$ are the classical steady-state Manning–Strickler formulas.

In order to solve this set of equations, we use a numerical procedure based on the following steps:

(i) Assuming that all values are known up to and including $n\Delta t$, the first equation allows us to predict the variable values h_p at time $(n+1)\Delta t$.

(ii) The second and third equations make it possible to predict the variables values r_p and s_p at time $(n+1)\Delta t$, taking into account the values $h^{t+\Delta t/2} = (h^t + h_p^{t+\Delta t})/2$, $\bar{u}^t$, $\bar{v}^t$, r^t and s^t known in the whole domain.

(iii) The fourth and fifth equations make it possible to compute the mean-averaged velocities $\bar{u}$ and $\bar{v}$ at time $(n+1)\Delta t$, taking into account the predicted values r_p and s_p.

(iv) The first two operations are repeated in order to improve the accuracy of the variables h, r and s, using the values r_p, s_p, $h^{t+\Delta t/2} = (h^t + h_p^{t+\Delta t})/2$, $\bar{u}^{t+\Delta t/2} = (\bar{u}^t + \bar{u}^{t+\Delta t})/2$ and $\bar{v}^{t+\Delta t/2} = (\bar{v}^t + \bar{v}^{t+\Delta t})/2$ known in the whole domain.

3.2. Development of the method

The finite element method is based on the approach of well-behaved functions, in the present case water-depth- and mean-averaged velocities, being defined over small regions of finite dimensions (called finite elements) into which the problem domain is subdivided.

If Δ^e is a generic element, the functions h, $\bar{u}$ and $\bar{v}$ are approximated within each element by:

$$h \approx \hat{h} = \sum_{i=1}^{n} N_i h_i,$$

$$\bar{u} \approx \hat{u} = \sum_{i=1}^{n} N_i \bar{u}_i,$$

$$\bar{v} \approx \hat{v} = \sum_{i=1}^{n} N_i \bar{v}_i,$$

where h_i, $\bar{u}_i$ and $\bar{v}_i$ are the function values at the nodal points and N_i represents linearly independent prescribed functions, usually polynomials.

Applying the weighted residual technique, Galerkin's procedure, for error minimization, we construct firstly the residual R_i; then, the approximate solution is selected in such a way that the weighting functions W_j are assumed to be equal to a combination of the shape functions N_i. Thus,

the error minimization equation is written as

$$\int_{\Delta^e} R_j W_j \, d\Delta^e = 0,$$

with $W_j = \sum_{i=1}^{n} N_i \delta\phi_i$, where $\delta\phi_i$ are arbitrary coefficients.

Applying the Galerkin method to the first residual R_1, which results from the continuity equation, we obtain

$$\begin{aligned}\int_{\Delta^e} R_1 W_1 \, d\Delta^e &= \int_{\Delta^e} R_1 N_i \delta\phi_i \, d\Delta^e \\ &= \int_{\Delta^e} (\hat{h}_t + \hat{h}\hat{u}_x + \hat{u}\hat{h}_x + \hat{h}\hat{v}_y + \hat{v}\hat{h}_y) N_i \delta\phi_i \, d\Delta^e \\ &= \int_{\Delta^e} N_i \Bigg[\sum_{j=1}^{n} N_j (h_j)_t + \sum_{k=1}^{n} (N_k)_x u_k \sum_{j=1}^{n} N_j h_j + \sum_{k=1}^{n} N_k u_k \sum_{j=1}^{n} (N_j)_x h_j \\ &\quad + \sum_{k=1}^{n} (N_k)_y v_k \sum_{j=1}^{n} N_j h_j + \sum_{k=1}^{n} N_k v_k \sum_{j=1}^{n} (N_j)_y h_j \Bigg] d\Delta^e = 0.\end{aligned}$$

These equations may be written in matrix form as follows:

$$A h_t + B h = 0, \tag{3}$$

with

$$a_{i,j} = \int_{\Delta^e} N_i N_j \, d\Delta^e, \qquad i, j = 1, n,$$

$$\begin{aligned}b_{i,j} &= \int_{\Delta^e} (N_k)_x u_k N_i N_j \, d\Delta^e + \int_{\Delta^e} N_k u_k N_i (N_j)_x \, d\Delta^e \\ &\quad + \int_{\Delta^e} (N_k)_y v_k N_i N_j \, d\Delta^e + \int_{\Delta^e} N_k v_k N_i (N_j)_y \, d\Delta^e, \qquad i, j, k = 1, n.\end{aligned}$$

The solution of equation system (3) provides the values of the nodal unknowns h_i. It may be solved using the following scheme:

$$A^t \frac{h^{t+\Delta t} - h^t}{\Delta t} + B^t [\alpha h^{t+\Delta t} + (1-\alpha) h^t] = 0$$

or

$$\left(\frac{1}{\alpha \Delta t} A^t + B^t \right) h^{t+\Delta t} = \frac{1}{\alpha \Delta t} A^t h^t - \frac{1-\alpha}{\alpha} B^t h^t,$$

with $0{\cdot}5 \leq \alpha < 1$.

The resulting matrix, although unsymmetric, is very sparse; so, we need to use an effective computer program for the solution of large, sparse and unsymmetric systems of linear equations as presented in Gupta and Tanji[8] or Hood.[9]

A similar sequence of calculations is performed for the remaining residuals R_2 to R_5, noting that the second derivatives can be reduced by one using integration by parts (or Green's theorem).

The boundary integrals resulting after application of the Green's theorem to reduce the second derivatives in the R_4 and R_5 residuals will only be needed if at least one of the element sides coincides with part of an external boundary with natural boundary conditions of the type $|\bar{V}|_n \neq 0$. Otherwise, it should not be considered.

The essential boundary conditions of the type $\bar{V}_j = V_{bj}$ may be introduced in the final system, after adding up the contributions from all elements and all sides with natural boundary conditions, by eliminating the rows corresponding to the prescribed unknowns and inserting the contributions of those prescribed unknowns on the right-hand side.

A variety of different elements may be used. However, here are used elements of the isoparametric family, which is a group of elements in which the shape functions are used to define the geometry as well as the depth-averaged velocity field.

We make use of the natural co-ordinate system (ξ, η) which allows us to use elements with curvilinear shapes. Therefore, an element of area $dx\,dy$ is calculated by the expression $dx\,dy = \det J\,d\xi\,d\eta$, where $\det J$ is the determinant of the Jacobian matrix J:

$$J = \begin{Bmatrix} \sum_{i=1}^{n} (N_i)_\xi x_i & \sum_{i=1}^{n} (N_i)_\xi y_i \\ \sum_{i=1}^{n} (N_i)_\eta x_i & \sum_{i=1}^{n} (N_i)_\eta y_i \end{Bmatrix},$$

which is evaluated, and its determinant, at the integration points.

In all such situations we have chosen a numerical three-point Gauss–Legendre quadrature to evaluate the one- and two-dimensional integrals in both ξ and η directions.

4. COMPUTATIONAL TESTS

4.1. Model comparisons with analytical solution

In order to validate the proposed numerical model, some experiments were performed and compared with the known analytical solution.

Figures 1 and 2 show two of these experiments. Both cases represent a solitary wave travelling along a horizontal no-friction rectangular channel of 100 m length. Numerical results are compared with the analytical solution for the solitary wave obtained by Boussinesq:[10]

$$h(x, t) = H + A\,\mathrm{sech}^2\{\sqrt{(3A/4H^3)}(x - \sqrt{[g(H+A)]}t) + x_0\},$$

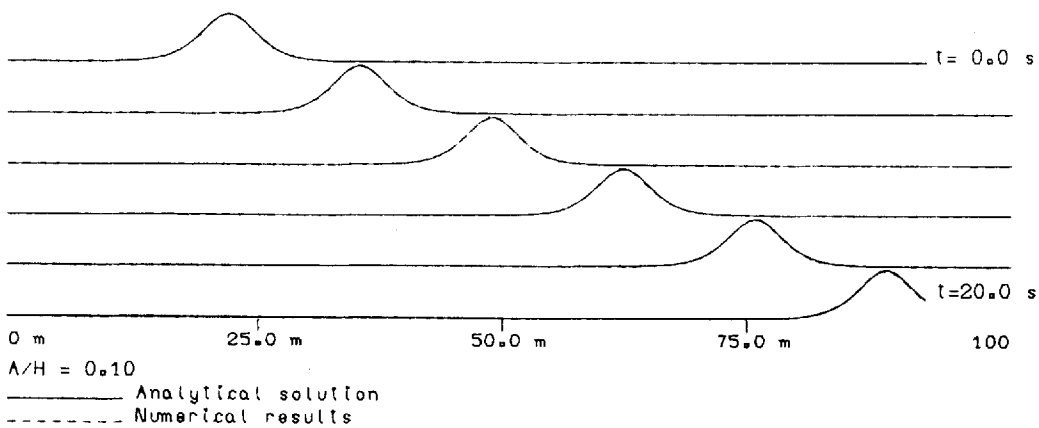

Figure 1. Solitary wave computation ($A/H = 0{\cdot}10$)

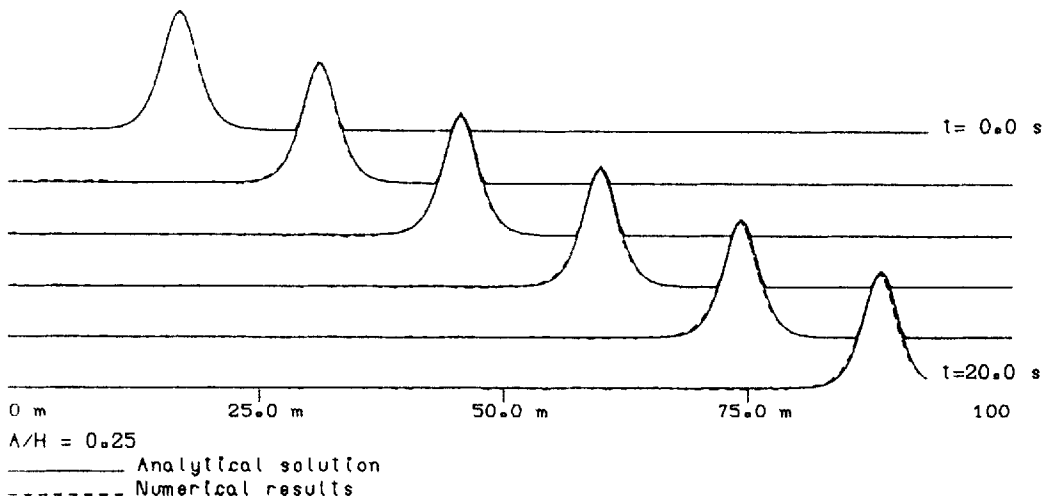

Figure 2. Solitary wave computation ($A/H = 0{\cdot}25$)

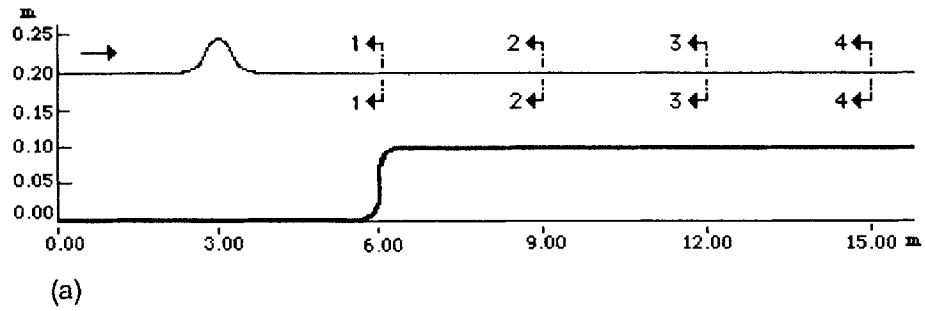

Figure 3(a). Installed depth gauges, bottom configuration and initial solitary wave position

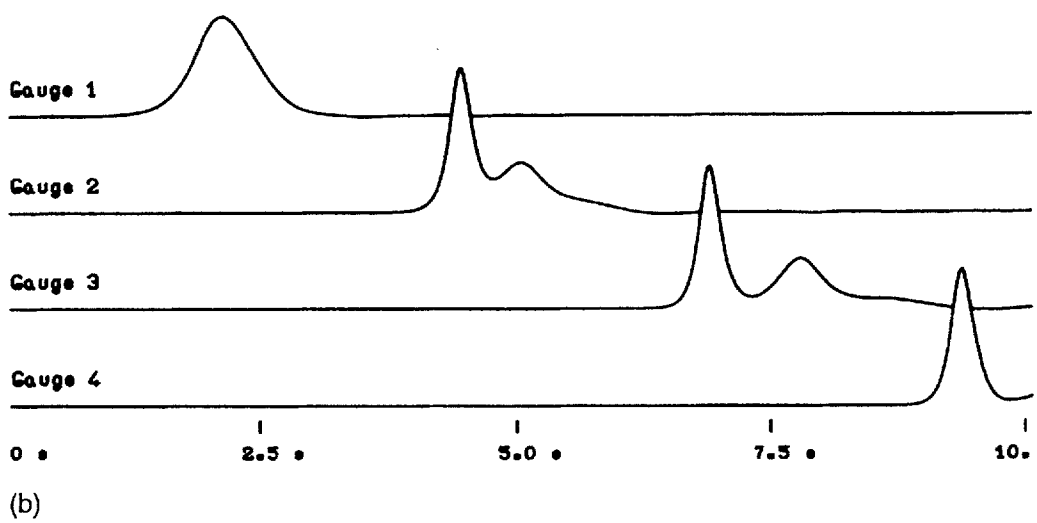

Figure 3(b). Solitary wave travelling over a step 0·10 m high ($0{\cdot}5H$). Numerical results for gauges 1–4

where A is the wave amplitude, $H = 1{\cdot}0$ m is the undisturbed water depth for $t = 0$ s and x_0 is the initial position of the crest ($x_0 = 22{\cdot}0$ m and $x_0 = 17{\cdot}0$ m for the first and second experiments, respectively). The channel was divided into eight-node quadrilateral elements of uniform length equal to 1·0 m.

The results shown in Figure 1 are for a wave with $A/H = 0{\cdot}10$, while Figure 2 shows the comparison for the ratio $A/H = 0{\cdot}25$. Both computations were carried out with $\Delta t = 0{\cdot}10$ s.

The agreement between the results obtained with the Boussinesq solution is perfect as much in wave amplitude as in phase for the ratio $A/H = 0{\cdot}10$; a slight loss in phase accuracy and in wave height is presented for the higher ratio $A/H = 0{\cdot}25$. Nevertheless, in both cases the dispersive waves are inconsiderable and the wave forms exhibit no important distortions.

4.2. Model comparisons with experimental data

In order to see the ability of the present numerical model to predict the effect in irregular bottom situations, the model has been applied to a solitary wave travelling along a two-level no-friction rectangular channel, having a step 0·10 m high located 6·0 m from the initial section. The channel was 15 m long and four depth gauges were located at 6·0, 9·0, 12·0 and 15·0 m from the initial section of the channel. For this situation a set of data measurements is available, performed by the authors at the 'Institut de Mécanique de Grenoble' (IMG), France.

Figure 3 shows the results for the following parameters:

wave amplitude, $A = 0{\cdot}0365$ m;
undisturbed water depth for $t = 0$ s, $H = 0{\cdot}20$ m before the step;
initial position of the crest wave, $x_0 = 3{\cdot}0$ m.

The results computed by this model show a good agreement with the measured data. In fact, the phase accuracy is perfect and the computational wave amplitudes recorded are the following:

first transmitted wave, $A_1 = 0{\cdot}0560$ m (0·0531 m);
second transmitted wave, $A_2 = 0{\cdot}0204$ m (0·0180 m);
third transmitted wave, $A_3 = 0{\cdot}0040$ m (0·0033 m)
(the experiment measured data in brackets).

Finally, two computational three-dimensional results are compared with the ones obtained experimentally, also performed by the authors at IMG. The first experiment consisted of a solitary wave overpassing a strait, as presented in Figure 4.

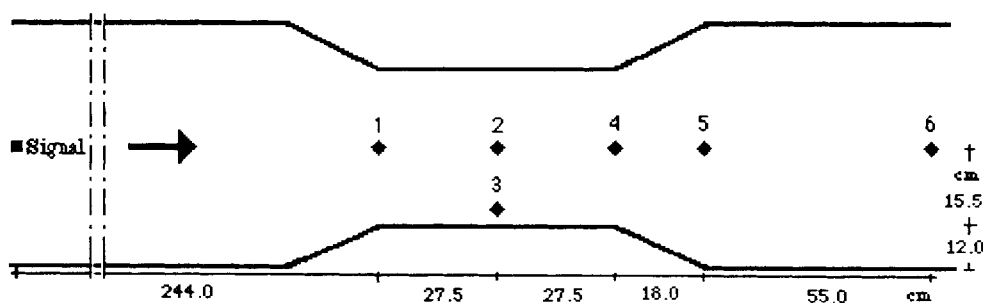

Figure 4. Model plan and installed depth gauges for a solitary wave overpassing a strait

The measuring and acquisition equipment employed was composed of six depth gauges connected to an acquisition system, which allowed each measuring channel to receive 50 values per second.

Five water surfaces computed at times $t_1 = 1{\cdot}0$ s, $t_2 = 1{\cdot}5$ s, $t_3 = 2{\cdot}0$ s, $t_4 = 2{\cdot}5$ s and $t_5 = 3{\cdot}0$ s are shown in Figure 5, where the closest wall of the channel was removed for better visualization. Figure 6 shows the comparison between the computed and measured results for the parameters:

undisturbed water depth, $H = 0{\cdot}15$ m;
wave amplitude, $A = 0{\cdot}0375$ m;

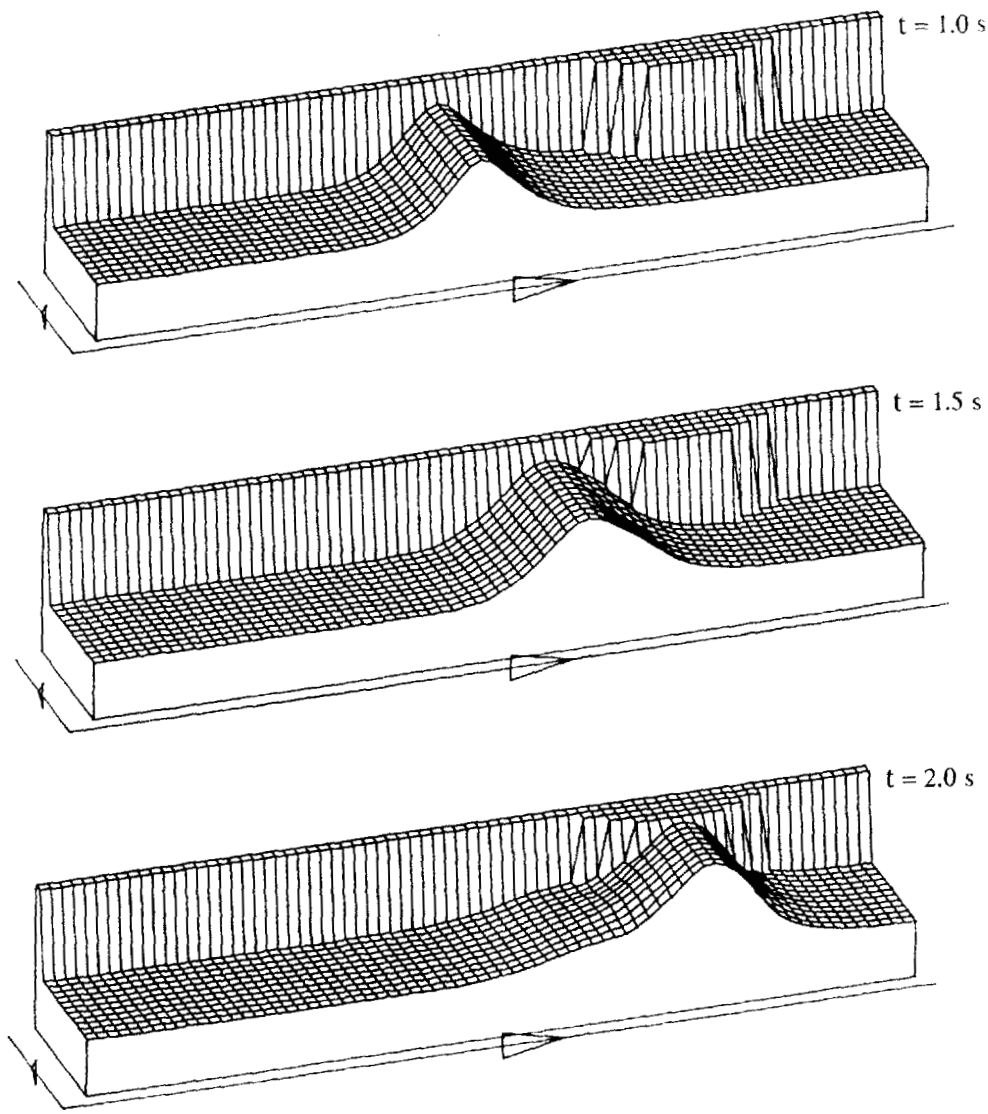

Figure 5. Three-dimensional perspective view of free-surface elevation for a solitary wave overpassing a strait, in time sequence. Vertical lines represent the farthest wall of the channel

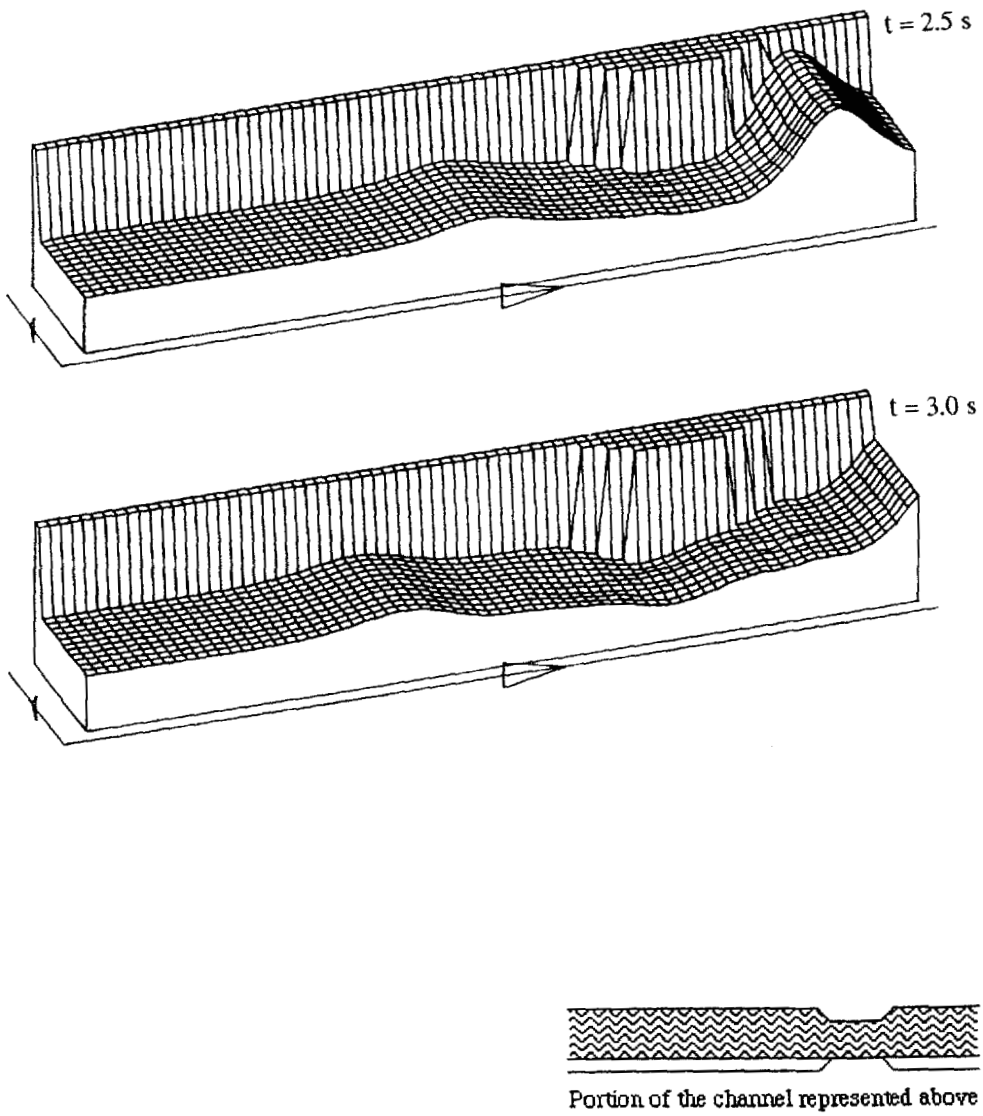

Figure 5. (Continued)

initial position of the crest wave, $x_0 = 1{\cdot}50$ m;
(x, y) co-ordinates of the six depth gauges (in metres): gauge 1 = (3·940, 0·275), gauge 2 = (4·215, 0·275), gauge 3 = (4·215, 0·150), gauge 4 = (4·490, 0·275), gauge 5 = (4·670, 0·275) and gauge 6 = (5·220, 0·275).

As we can see, the results are in good agreement both for wave height and for phase accuracy.

The second experiment consisted of a solitary wave overpassing a vertical circular cylinder. This is done in a channel 0·55 m wide. The cylinder, with 16 cm of diameter, is held fixed symmetrically in the centre of a channel and pierces the free surface (Figure 7).

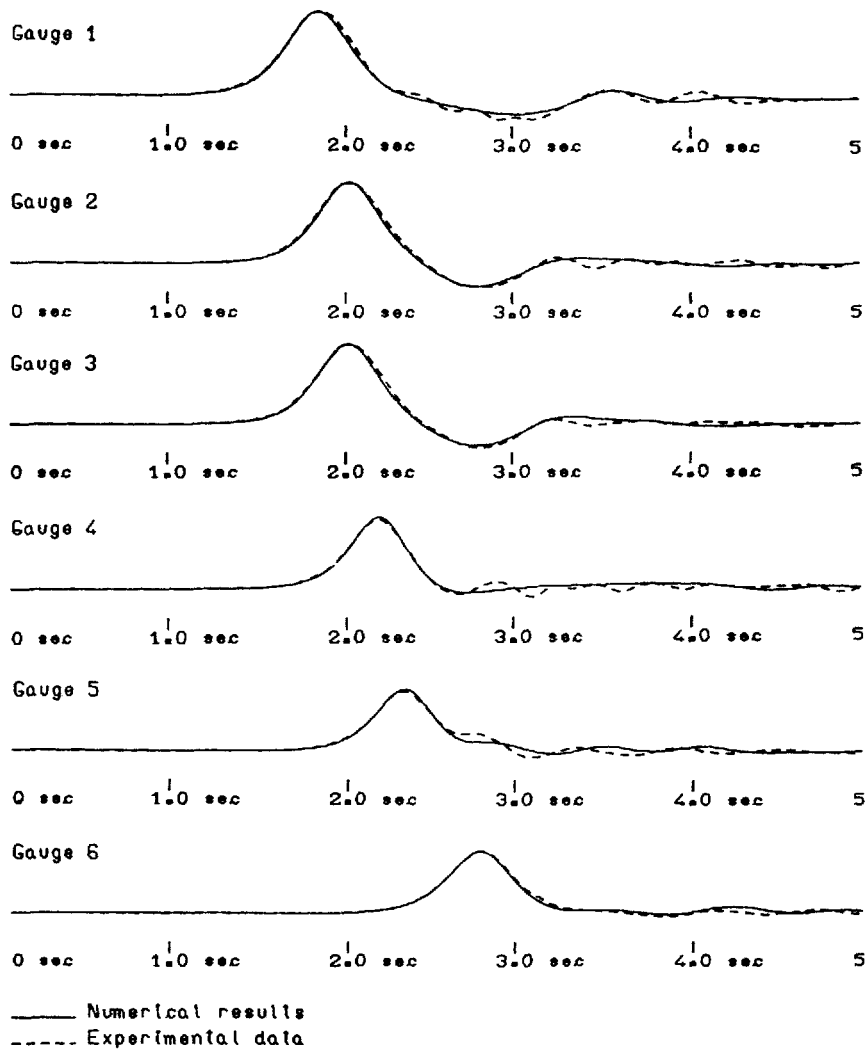

Figure 6. Comparison between numerical and experimental results for a solitary wave overpassing a strait

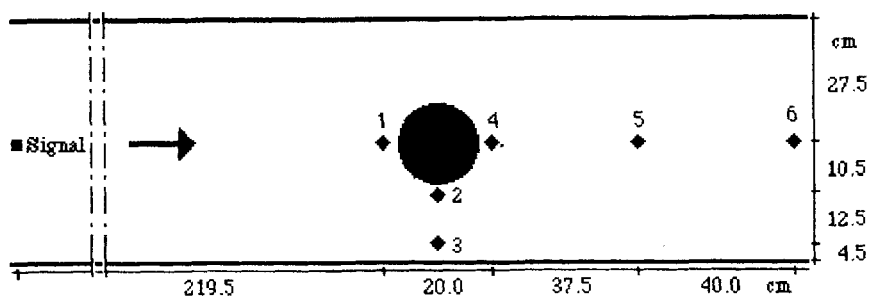

Figure 7. Model plan and installed depth gauges for a solitary wave overpassing a vertical circular cylinder

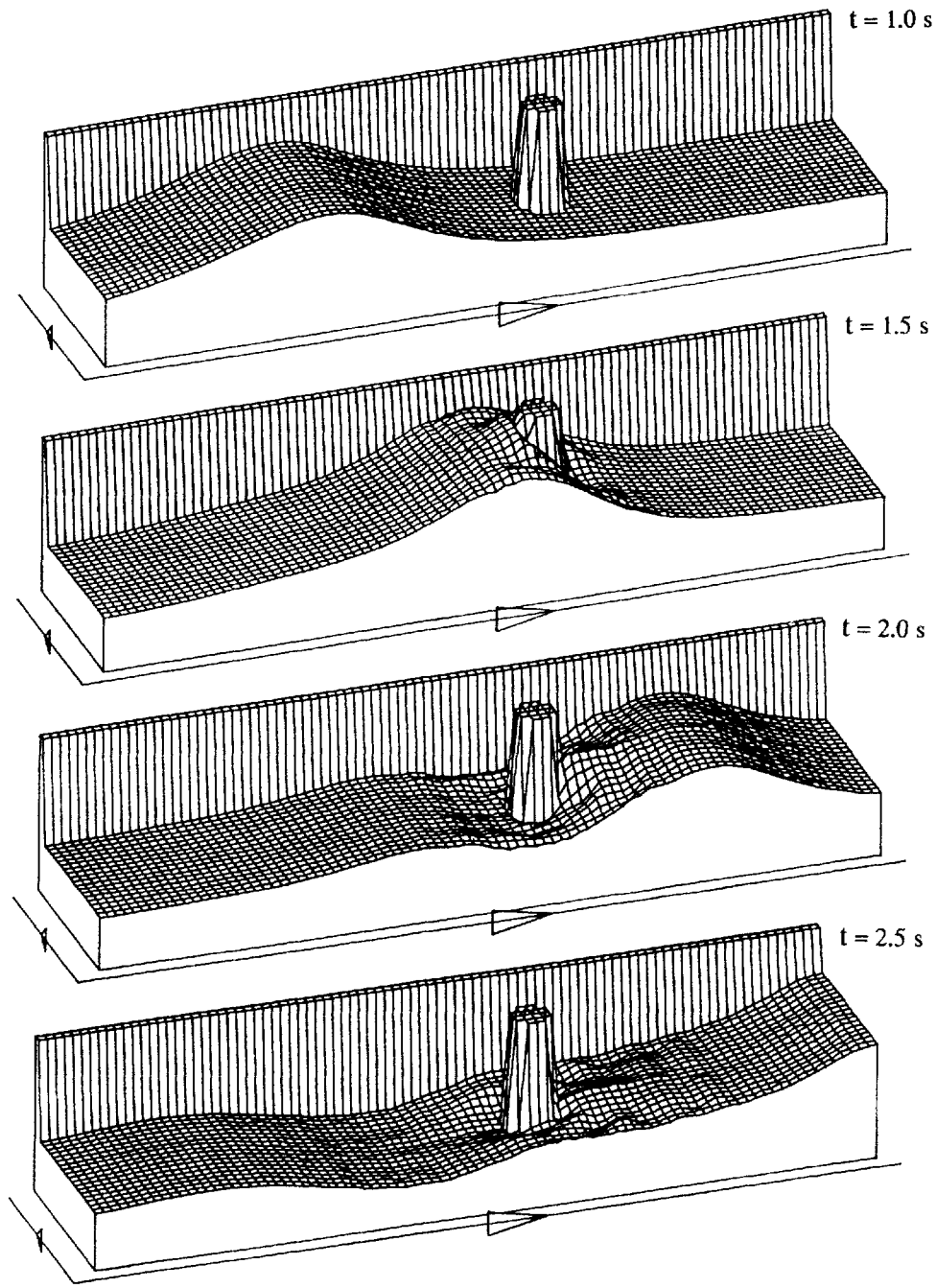

Figure 8. Three-dimensional perspective view of free-surface elevation for a solitary wave overpassing a vertical circular cylinder, in time sequence. Vertical lines represent the cylinder and the farthest wall of the channel

We have employed six depth gauges located at the (x, y) co-ordinates (in metres): gauge 1 = (4.220, 0·275), gauge 2 = (4·320, 0·170), gauge 3 = (4·320, 0·045), gauge 4 = (4·420, 0·275), gauge 5 = (4·795, 0·275) and gauge 6 = (5·195, 0·275). Figure 8 shows four half portions of the domain at times $t_1 = 1{\cdot}0$ s, $t_2 = 1{\cdot}5$ s, $t_3 = 2{\cdot}0$ s and $t_4 = 2{\cdot}5$ s for the following parameters:

undisturbed water depth, $H = 0{\cdot}15$ m;
wave amplitude, $A = 0{\cdot}0375$ m;
initial position of the crest wave, $x_0 = 2{\cdot}025$ m.

As was the case in Figure 5, the closest wall of the channel was also removed.
The comparison between the computed and measured results is presented in Figure 9.

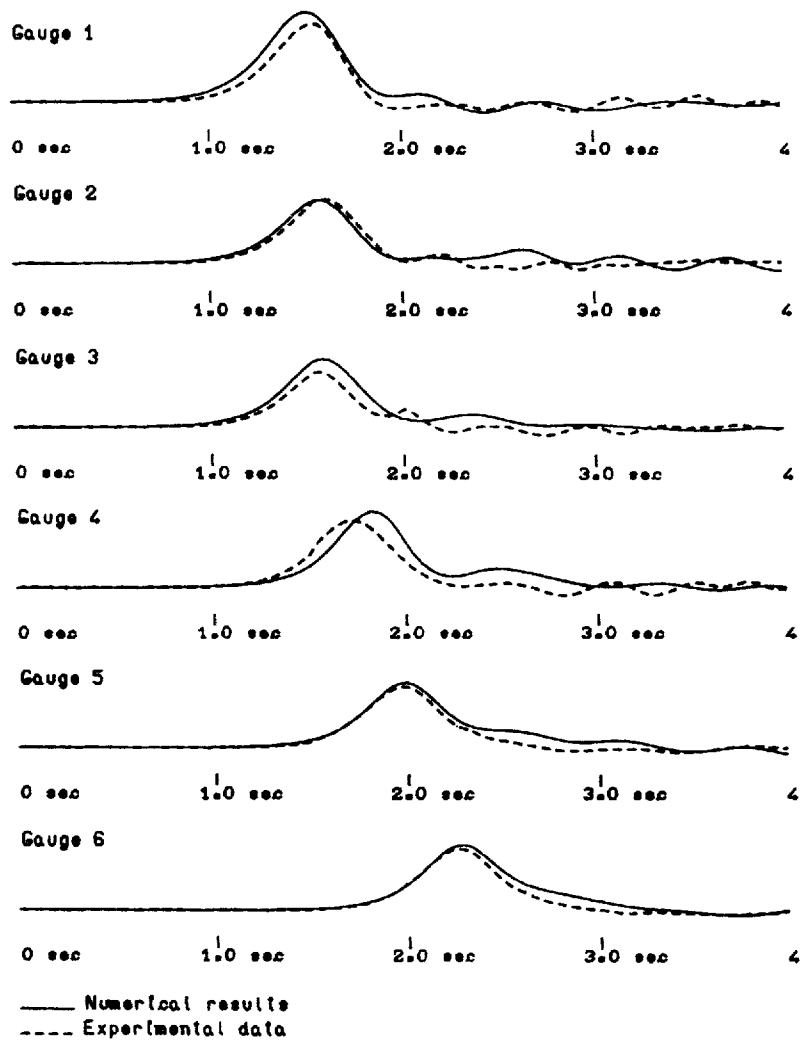

Figure 9. Comparison between numerical and experimental results for a solitary wave overpassing a vertical circular cylinder

Excluding the gauge immediately behind the cylinder, which is not understandably good (the motion is assumed irrotational), the others agreed reasonably with measured data.

5. CONCLUSIONS

The developed model permits simulation of wave propagation in shallow-water conditions whenever the ratio A/H is not very high ($A/H \leq 0{\cdot}4$–$0{\cdot}5$); this limitation follows basically from the Boussinesq-type equations, and not so much from the numerical method used.[11]

The model can be employed in any geometry, under complicated boundary conditions, and with arbitrary bathymetry, without any additional computational effort.

The accuracy of the developed model seems to be, for the same equations, higher than explicit finite-difference models and it only sustains comparison with implicit finite-difference models.

The comparison between this model with a finite-difference one, both in one space dimension and utilizing the same numerical procedure described in Section 3.1, shows that the finite-difference model is 3 to 4 times faster than the present one, for the same precision. However, despite requiring more computational effort, in practical treatment of real situations (arbitrary geometry, important bathymetric irregularity, different local resolution of the computational grid, etc.) this inconvenience is frequently overshot because less points are normally necessary.

ACKNOWLEDGEMENTS

The authors gratefully acknowledge A. Temperville (IMG) for his valuable collaboration, and the financial support from JNICT, Portugal.

REFERENCES

1. D. R. Basco, 'Limitations of the Saint-Venant equations in dam-break analysis', *J. Hydraul. Eng.*, **114**(7), 950–965 (1989).
2. A. M. Gharangik and M. H. Chaudry, 'Numerical simulation of hydraulic jump', *J. Hydraul. Eng.*, **117**(9), 1195–1210 (1991).
3. G. Pedersen and B. Gjevik, 'Run-up of solitary waves', *J. Fluid Mech.*, **27**, 815–827 (1983).
4. D. H. Peregrine, 'Calculations of the development of an ondular bore', *J. Fluid Mech.*, **25**, Part 2, 321–330 (1966).
5. D. H. Peregrine, 'Long waves on a beach', *J. Fluid Mech.*, **27**, 815–827 (1967).
6. N. D. Katopodes and Chien-Tai Wu, 'Computation of finite-amplitude dispersive waves', *J. Waterway, Port, Coastal and Ocean Eng.*, **113**(4), 327–346 (1987).
7. S. K. Gupta and K. K. Tanji, 'Computer program for solution of large, sparse, unsymmetric systems of linear equations', *Int. j. numer. methods eng.*, **11**, 1251–1259 (1977).
8. P. Hood, 'Frontal solution program for unsymmetric matrices', *Int. j. numer. methods eng.*, **10**, 379–399 (1976).
9. J. Boussinesq, 'Théorie des ondes et des remous qui se propagent le long d'un canal rectangulaire horizontal', *L. Math. Pure et Appl.*, **2**(17), 55–108 (1872).
10. F. J. Seabra Santos, D. P. Renouard and A. M. Temperville, 'Étude théorique et expérimentale des domaines de validité des théories d'évolution des ondes en eau peu profonde', *Ann. Geophys.*, **6**(6), 671–680 (1988).
11. F. J. Seabra Santos, 'Wu and Green & Naghdi approximations in the framework of the shallow-water theory', 4º Simpósio Luso-Brasileiro de Hidráulica e Recursos Hídricos, LNEC, Lisboa, Portugal.